USB Proceedings

2014 International Conference on Electrical Machines (ICEM)

Andel`s Hotel Berlin
Berlin, Germany
02 - 05 September, 2014

Sponsored by

The Institute of Electrical and Electronics Engineers (IEEE)
IEEE Industrial Electronics Society (IES)

Co-sponsored by

ETG - Power Engineering Society withing VDI

Permanent Magnet Synchronous Reluctance Machine - Design guidelines to improve the acoustic behavior

S. Rick, A. K. Putri, D. Franck and K. Hameyer
Institute of Electrical Machines
RWTH Aachen University
Email: sebastian.rick@iem.rwth-aachen.de

***Abstract*—The permanent magnet synchronous reluctance machine (PMSynRM) is a type of permanent magnet synchronous machine (PMSM) with the objective to provide high reluctance torque. This is realized by a particularly designed constellation of flux barriers in the rotor of the machine. Beside high efficiency and supplied power density, an acoustic evaluation of this machine is performed for various applications, for example in hybrid and electric vehicles (HEV, EV). A study for the acoustic design of a PMSynRM is presented in this paper. An approach to improve the magnetic circuit by varying the shape of the flux barriers is introduced. Using numerical simulations every operating point in the d-q-diagram is considered. The local force density in the air gap of the machine is calculated and analyzed with a 2-D Fourier Transformation. The results are used as analysis criterion.**

***Index Terms*—permanent magnet synchronous machine, reluctance torque, flux barrier, acoustic design, force density.**

I. Nomenclature

Table I
Nomenclature.

symbol	quantity	unit	description
A	-	-	coefficient for harmonic distortion
B_{gap}	-	T	magnetic air gap flux density
γ_{mech}	0 - 90	$^\circ\,(deg)$	position angle in the air gap
$d_{\mathrm{fp,b}}$	-	mm	flux path width at bridges
$d_{\mathrm{fp,c}}$	-	mm	flux path width at barrier corner
$d_{\mathrm{fp,m}}$	-	mm	flux path width at magnets
$F_{\mathrm{a,rad}}$	-	N/m^2	radial force density
i_{d}	0 - 100	A	d-current
i_{q}	0 - 100	A	q-current
I	0 - 100	A	sinusoidal peak current
k	0-1	-	total harmonic distortion
p	4	-	pole pairs
ψ	0 - 90	$^\circ\,(deg)$	control angle
θ_{i}	varied	$^\circ\,(deg)$	inner flux barrier angle
θ_{a}	varied	$^\circ\,(deg)$	outer flux barrier angle
w_{b1}	-	mm	width of barrier 1

II. Introduction

To describe the acoustic behavior of electrical machines, an expansion of electromotive forces through the drive train of the system is necessary. Electric energy is stored in the battery

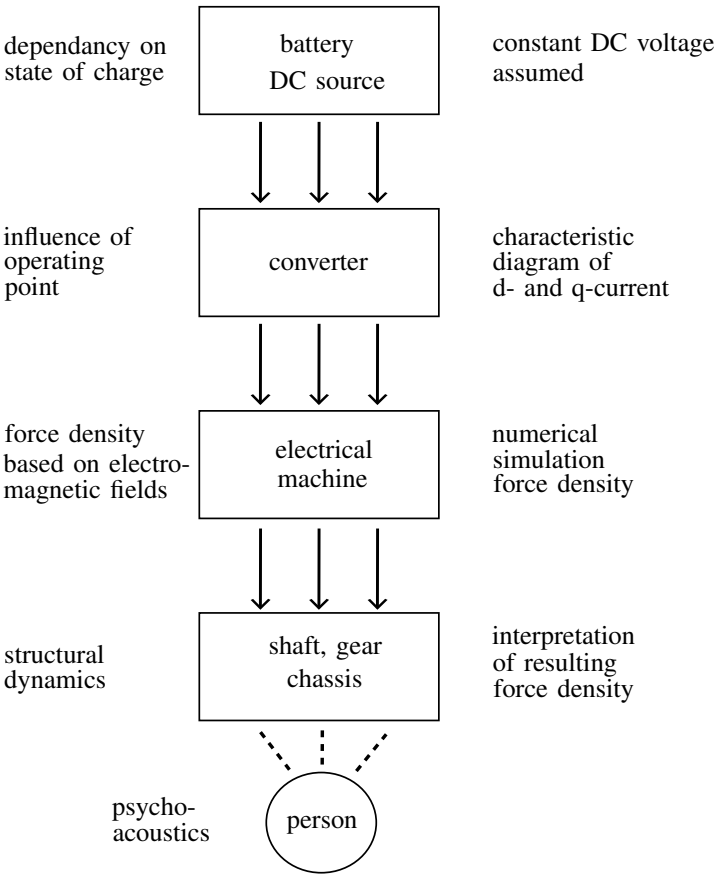

Figure 1. Structure diagram of components of a drive train. Left side: description of relevant processes that influence the acoustic behavior of a drive train. Right side: Considered effects in the here presented model.

and provided to the machine by electronic power converters. The electrical machine produces radial, tangential and axial forces, which are transferred through the drive shaft, gear and chassis of the vehicle. The paper is based on a model of a drive train, which consists of the four parts, the battery, converter, electrical machine and mechanical gear. In the following the four parts of this model are introduced. A summary of this model is shown in figure 1.

The battery storage system provides electrical energy by DC voltage. To simulate such a system in a test bench, a

978-1-4799-4775-1/14/$31.00 ©2014 IEEE

DC-system consisting of rectifiers and converters is used [1]. By rectifying a sinusoidal 3-phase AC voltage a DC voltage is realized. In the rectifying process of the AC to DC current harmonic disturbance is generated. This disturbance propagates to the electrical machine through the DC - AC converter, resulting in harmonics in the force density. Such effects have to be included in the modeling process. A relevant parameter is the switching frequency of the semiconductor device. However, for the presented simulations this effect is neglected due to simplicity. The control of the 3-phase PMSynRM is realized by the converter system. The two axis transformation is used to transform the 3-phase stationary AC system into an equivalent two phase rotating system with perpendicularly oriented axis. The transformed two currents i_d and i_q are parameters for the possible operating points. The PWM switching process and therefore the corresponding frequency causes harmonics in the motor‘s current, which then generate harmonics in the force density of the PMSynRM. There are different approaches to reduce single tones, for instance by a randomly modulated PWM [2][3]. We focus for the evaluations on the appropriate operating points described by i_d and i_q, which are considered as variable parameters.

In this paper we focus on the acoustic analysis of the electrical machine. There are the construction caused parametric harmonics, for instance slotting effects, effect of eccentricity and magnetic saturation [4][5]. On the other hand the electrical machine is influenced by the converter on the one side and the mechanical gear on the other side. This results in a bidirectional acoustic coupling effect, which determines harmonics in the machine. The produced forces in the air gap, which are excited by electromagnetic fields, cause a time and spatial dependent deformation of the material in the stator [6]. This results in air-borne and structure-borne sound. To analyze the acoustic behavior of the machine the force excitation is distinguished by radial and tangential force components [7]. The machine is un-skewed. For this reason the axial force components are neglected. A 2D model is applied for the simulations. By evaluation of the resulting force density the source for the excited noise can be identified. There are different design options to improve the acoustic behavior of a machine, for example by skewing the stator or rotor or by variating the winding [8]. In this paper a construction variation of the flux barriers in the rotor geometry is studied [9].

The resulting force densities excite the structure of the stator teeth [10]. On the one hand the resulting deformation propagates to the machine housing and excites the ambient air, which leads to air-borne sound. On the other hand the vibration is transferred to other nearby components of the drive train, for instance the gear, bearings or chassis. This is described by the structure-borne sound. An analytical model is used to calculated the surface velocity of the machine housing to identify the acoustic emission of the machine. In a final step of this analysis this surface velocity is used for a psycho acoustic evaluation, which is not part of this paper.

III. Machine design and modeling

The considered topology of a PMSynRM consists of two layers of flux barriers in the rotor, as shown in figure 2 [11][12]. Parameters of the upper, smaller flux barrier are subscripted with a ”1”, these of the lower larger flux barrier with a ”2”. In the center part of the flux barrier a permanent magnet is placed, the side parts are filled with air. The small bridges at the end of each flux barrier are configured to provide an appropriate compromise between ”small amount of leakage flux” (small and thin bridge) and ”high mechanical stability” (large and wide bridge) [9][13].

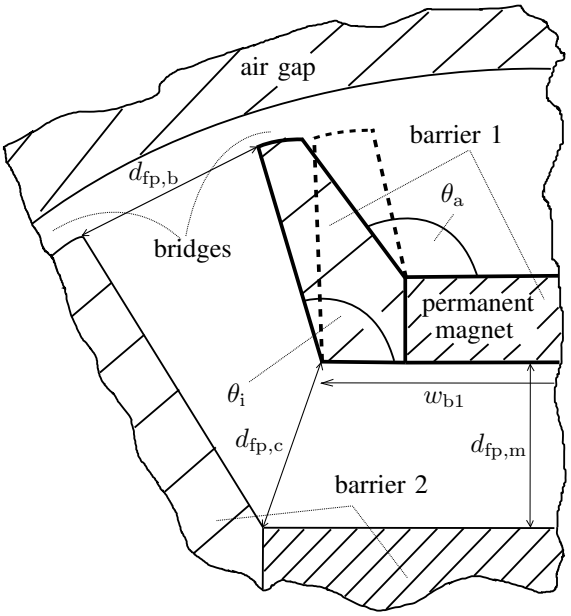

Figure 2. Cross section of a two layer PMSynRM rotor (2*p*=8). Relevant dimensions for simulation of parameter variation in barrier 1. Shape of Barrier 2 and bridge widths are kept constant.

The presented approach for designing a machine is intended for a general design strategy of PMSynRMs. The chosen dimension of parameters is adapted to machines in a medium power range, for example for automotive applications. The design of the winding and the skewing of the stator or rotor is not considered. This gives the opportunity to keep track of individual design aspects and their influence on the behavior of the machine. In a two layer PMSynRM the position of the larger and deeper buried layer has a significant influence to the resulting torque [9]. This paper focuses on acoustic behavior. In this analysis the shape of barrier 2 is kept constant. Thereby the width of barrier 1 w_{b1}, the flux path width between the permanent magnets $d_{\mathrm{fp,m}}$ and the flux path width at the barrier corners $d_{\mathrm{fp,c}}$ remains constant.

The first two considered parameters are the flux barrier angles θ_i and θ_a of barrier 1 (figure 2). It is important to analyze their effects in combination, due to their geometric connection. By widening both flux barrier angles the position of the bridges and the width of the poles is increased. By enlarging the inner barrier angle θ_i and simultaneously keeping the outer barrier angle θ_a constant, the width of the flux barrier is changed. A parameter study for different variants of these two barrier angles of the first barrier is performed and their implications are interpreted in the next sections.

A further aspect which is studied is the adjusted operating point in the control of the machine. The operating point is

Table II
PARAMETER STUDY.

description	symbol	unit	quantity
inner flux barrier angle	θ_i	$^\circ\,(deg)$	100, 110, ..., 150, 160
outer flux barrier angle	θ_a	$^\circ\,(deg)$	θ_i-10,θ_i-5,θ_i+5,θ_i+10
sinusoidal peak current	I	A	0, 5, 10, ..., 95, 100
control angle	ψ	$^\circ\,(deg)$	0, 5, 10, ..., 85, 90

described by the value of the appropriate current I and the control angle ψ. They are both displayed in a complex d- and q-plane. The parameter study is arranged along the whole range of possible operating points and specific operating points are observed, to interpret their influence on the behavior of the machine.

The simulation is performed using 2D finite element analysis (FEA) with focus on force density calculations.

The radial and tangential force density acting on the stator is being calculated on the interface between the stator core and the air gap and coils respectively. The forces can be approximated based on the air gap field, therefore the magnetic flux density in the air gap B_gap is analyzed in section IV. The resulting torque is analyzed in section V [14]. The radial force density is observed in section VI.

IV. EVALUATION OF AIR GAP FLUX DENSITY

In this section the magnetic flux density in the air gap B_gap of the PMSynRM is analyzed [15]. For each constellation of flux barrier angles θ_i and θ_a in table II, a numerical simulation is performed. To compare the behavior of the air gap flux density, the time and spatial development is considered. Considering the symmetric conditions of the model, a 90° mechanical cutout was selected for simulation. The rotation is performed in 180 steps with a step width of 0.5° mechanical. For the spatial evaluation the first simulation step is chosen as reference. In figure 3 the spatial behavior of the air gap flux density is shown. The inner flux barrier angle θ_i is kept constant at 160°. This represents the widest constellation of the parameter study at this flux barrier. The

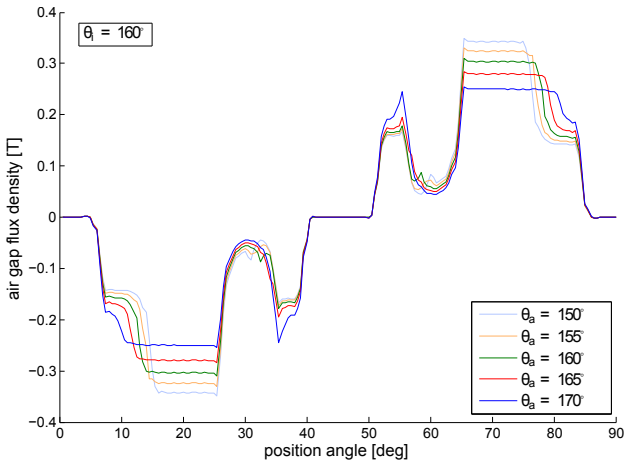

Figure 3. Air gap flux density. Spatial behavior. Inner flux barrier angle $\theta_\mathrm{i} = 160°$. Simulation process along one pole pair (90°).

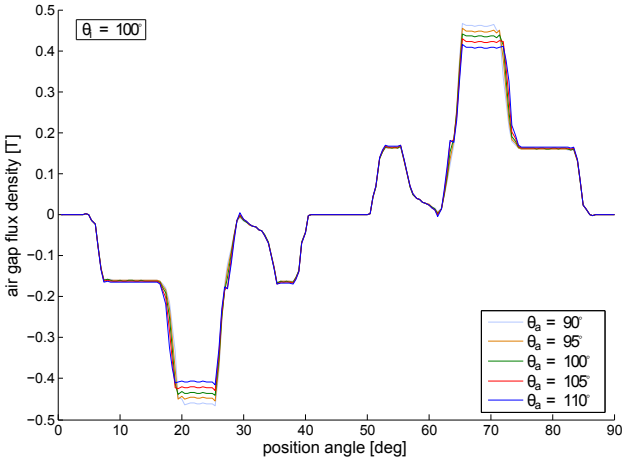

Figure 4. Air gap flux density. Spatial behavior. Inner flux barrier angle $\theta_\mathrm{i} = 100°$. Simulation process along one pole pair (90°).

outer flux barrier angle θ_a is varied, what results in different lengths of the flux barrier bridges and different widths of the barriers. It is observable that the magnetic flux peak at position angle $\gamma = 55°$ is increased with larger θ_a. In this case the length of the bridge of barrier 1 is getting shorter and thereby the flux is concentrated in a smaller area. The level of the plateau at position angle $\gamma_\mathrm{mech} = 70°$, which represents a position at the bridge of the barrier, decreases. It is also shown, that the length of the plateau is increased with larger θ_a, which changes the shape of the air gap flux density.

In figure 4 the behavior of the air gap flux density B_gap is shown for the inner flux barrier angle $\theta_\mathrm{i} = 100°$, which is the smallest simulated width of flux barrier 1. The difference in the shape of the curve, according to different outer flux barrier angles θ_a, is small in comparison to figure 3. In the plateau position at $\gamma_\mathrm{mech} = 70°$ a small difference is visible.

To interpret the influence of every constellation of flux barrier angles θ_i and θ_a, the total harmonic distortion (THD)

$$k = \sqrt{\frac{A_2^2 + A_3^2 + A_4^2 + ...}{A_1^2 + A_2^2 + A_3^2 + A_4^2 + ...}} \qquad (1)$$

is calculated. The coefficients A describe the time-averaged spatial harmonics of the air gap flux density B_gap. Their index characterizes the specific spatial order and thereby the index "1" represents the fundamental wave. A small harmonic distortion is required to realize an adequate electromagnetic force transformation in the air gap and to lower torque ripple

Table III
TOTAL HARMONIC DISTORTION (THD).

θ_a [°]	θ_i [°]						
	100	110	120	130	140	150	160
-10	0.491	0.482	0.471	0.461	0.448	0.433	0.419
-5	0.485	0.476	0.466	0.455	0.441	0.424	0.407
0	0.479	0.470	0.460	0.448	0.433	0.414	0.398
5	0.472	0.464	0.454	0.441	0.424	0.405	0.396
10	0.464	0.457	0.447	0.433	0.414	0.398	0.408

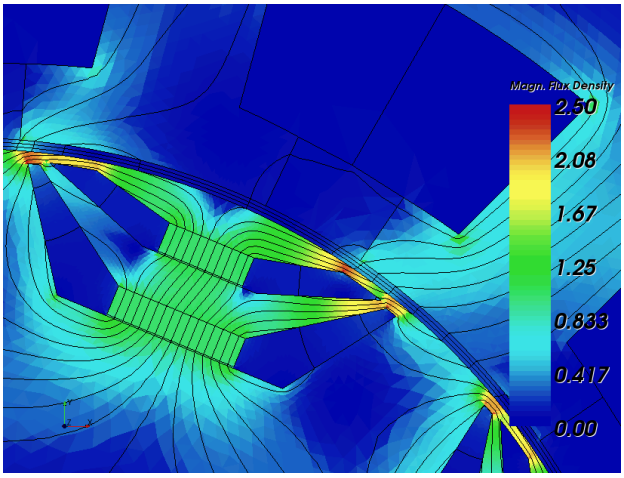

Figure 5. Magnetic flux density simulation. Inner flux barrier angle $\theta_\mathrm{i} = 160°$. Outer flux barrier angle $\theta_\mathrm{a} = 165°$. Constellation with lowest harmonic distortion k.

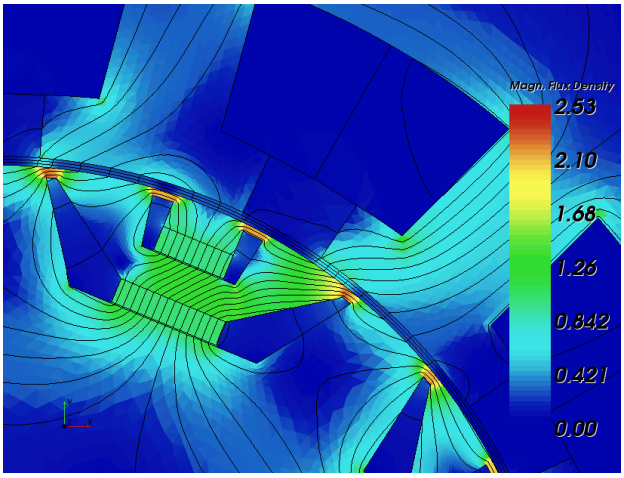

Figure 6. Magnetic flux density simulation. Inner flux barrier angle $\theta_\mathrm{i} = 100°$. Outer flux barrier angle $\theta_\mathrm{a} = 90°$. Constellation with highest harmonic distortion k.

and disturbing radial force densities. The variation is simulated as described in table II and the outer flux barrier angle θ_a is considered relatively to the inner flux barrier angle θ_i.

In table III the total harmonic distortion k for every angles' constellation of the first barrier is shown. The highest harmonic distortion in this table appears for the constellation ($\theta_\mathrm{i} = 100°$ / $\theta_\mathrm{a} = 90°$), the smallest for the constellation ($\theta_\mathrm{i} = 160°$ / $\theta_\mathrm{a} = 165°$). The constellation ($\theta_\mathrm{i} = 160°$ / $\theta_\mathrm{a} = 170°$) in table III causes a higher harmonic distortion. Leakage flux at the bridges results in saturation effects which leads to a larger peak in the air gap flux density (compare figure 3 at $\gamma = 55°$). From this it follows that a wide opened flux barrier, which is getting larger form the center to the bridges, results in lesser disturbing harmonics in the air gap flux density and therefore a better acoustic behavior. A smaller bridge width also reduces the mechanical stress, which is beneficial for the mechanical design of the rotor of the machine [9].

In figure 5 and figure 6 the magnetic flux density for the first simulation step of two different flux barrier angle constellations is shown. The constellation in figure 5 has the widest flux barrier and a slightly pointed shape of the side pockets. This constellation has a very similar cross section towards a typical PMSM with one layer buried magnets, due to the closeness of the two bridges of the two flux barriers. The flux path width at the bridges $d_\mathrm{fp,b}$ (figure 2) is very small when compared to the flux path width at the corner $d_\mathrm{fp,c}$, which reduces the reluctance torque of the machine. This aspect will be considered in section V. The flux barrier angle constellation in figure 6 has the smallest flux barrier width of all simulated models and the shape of each pocket is wider in the area of the bridges. The bridge of barrier 1 produces a higher flux density with shorter plateau. This is shown in figure 4 at position angle $\gamma = 70°$. The evaluation in table III shows, that the width of the pockets of each barrier has less influence on the harmonic distortion, compared to the position of the bridges. The difference between the most and the least advantageous constellation is 20%.

V. Evaluation of Torque

In this section the resulting torque of the machine is considered. The provided total inner torque of this machine design is calculated and analyzed. The torque behavior is considered for different operating points. Therefore a numerical simulation is executed for an i_d-i_q-plane to examine every possible operating point. In the next subsection the torque ripple is regarded. In the second subsection the higher harmonics behavior of the torque is considered for different operating points.

In table IV the resulting torque of the machine for different flux barrier angles θ_i and θ_a is shown. The maximum torque is provided at $\theta_\mathrm{i} = 150°$ and $\theta_\mathrm{a} = 140°$. By increasing θ_i from 150° to 160° the flux path between barrier 1 and 2 gets very thin, what reduces the established reluctance torque and therefore the resulting total torque (compare figure 5). By decreasing θ_i, the produced permanent magnet flux in the center of the barrier can not be conducted to the stator as good as before, what causes a decreasing torque. By increasing the outer flux barrier angle θ_a the shape of the barrier gets sharper to the bridges and the leakage flux increases. Therefore the resulting torque also decreases.

Table IV
TORQUE [NM].

θ_a [°]	θ_i[°] 100	110	120	130	140	150	160
-10	7.895	8.002	8.089	8.167	8.232	8.242	8.052
-5	7.894	7.998	8.086	8.163	8.226	8.235	8.047
0	7.887	7.992	8.078	8.153	8.213	8.216	8.013
5	7.874	7.980	8.067	8.138	8.190	8.177	7.926
10	7.853	7.962	8.047	8.113	8.150	8.101	7.746

As evaluation parameters of the torque ripple the resulting torque in an inner flux barrier angle θ_i must be constant and independent of the change in the flux barrier angle θ_a. In table V the variation in torque for changing the flux barrier angle θ_a is calculated. Therefore the maximum and the minimum torque value is referenced to the arithmetic mean of

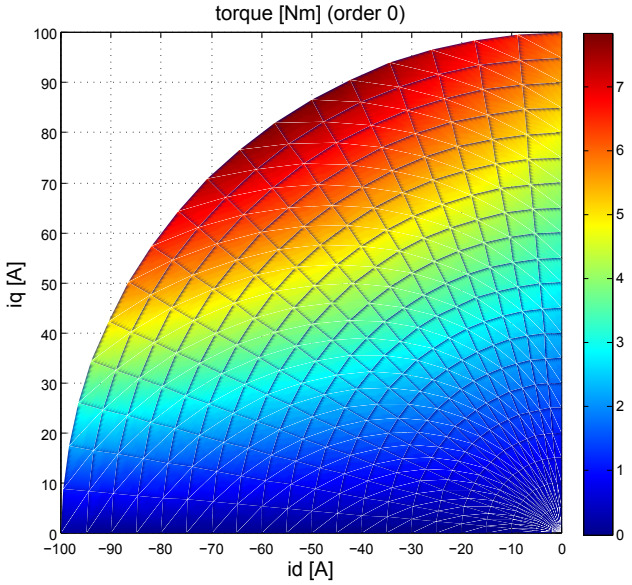

Figure 7. Fundamental wave of torque as a function of currents i_d and i_q. Parameter constellation with $\theta_\mathrm{i} = 100°$ and $\theta_\mathrm{a} = 110°$.

every torque with the same θ_i. The variation of torque for flux barrier angle $\theta_\mathrm{i} = 160°$ is much higher than in other cases, which results in an increasing reduction of reluctance torque. This is explained by the thinner flux path width at the bridges $d_\mathrm{fp,b}$ which leads to higher saturation in the magnetic flux in this area. Therefore the most beneficial constellation, which is considered in further sections, is for the flux barrier angle $\theta_\mathrm{i} = 150°$, which results in the highest output torque. The torque variation concerning other inner barrier angles θ_i is less than 4%, which is sufficient for further interpretations.

The acoustic behavior of the PMSynRM changes dependent on its operating points. Therefore parameter variations for the amplitude of the current I and the control angle ψ is conducted. Variation details are shown in table II. In figure 8 the amplitude of the fundamental wave of the torque is shown as a function of the currents i_d and i_q. The control angle should be set to $\psi = 35°$ to reach maximum torque per ampere (MTPA) for the nominal torque of the machine.

A. Torque ripple

In this subsection the torque ripple of the PMSynRM is calculated. Table VI shows the resulting torque ripple for the parameter variation of table II with different flux barrier angles θ_i and θ_a. An advantageous constellation is a large inner flux barrier angle θ_i and the outer flux barrier angle θ_a should be slightly larger to ensure a pointed shape of the side of the barrier. A spire shape is also beneficial for the mechanical stability in the bridges of the barrier [9].

Table V
VARIATION OF TORQUE [%].

θ_a [°]	θ_i[°] 100	110	120	130	140	150	160
-10	0.2	0.2	0.2	0.2	0.4	0.6	1.2
10	0.4	0.3	0.3	0.4	0.6	1.1	2.6

Table VI
TORQUE RIPPLE.

θ_a [°]	θ_i[°] 100	110	120	130	140	150	160
-10	1.793	1.570	1.275	0.942	0.597	0.264	0.021
-5	1.649	1.418	1.114	0.777	0.434	0.119	0.107
0	1.502	1.264	0.953	0.614	0.278	0.002	0.132
5	1.347	1.105	0.792	0.456	0.136	0.084	0.082
10	1.189	0.946	0.632	0.303	0.019	0.109	0.028

Table VII
TORQUE RIPPLE REFERRED TO TORQUE [%].

θ_a [°]	θ_i[°] 100	110	120	130	140	150	160
-10	22.7	19.6	15.8	11.5	7.3	3.2	0.3
-5	20.9	17.7	13.8	9.5	5.3	1.4	1.3
0	19.0	15.8	11.8	7.5	3.4	0.02	1.6
5	17.1	13.8	9.8	5.6	1.7	1.0	1.0
10	15.1	11.9	7.9	3.7	0.2	1.3	0.4

In table VII the torque ripple is referenced to the resulting mean torque of the machine. The best constellation is with flux barrier angle $\theta_\mathrm{i} = 150°$ and $\theta_\mathrm{a} = 150°$.

The results of this analysis are: the inner barrier angle θ_i should be wide to reduce the torque ripple and the outer barrier angle θ_a has only small influence to the behavior of the torque ripple. For smaller angle θ_i the outer barrier angle θ_a should be designed slightly larger than θ_i to achieve a pointed shape of the barrier.

B. Evaluation of different operating points

In this section torque harmonics are evaluated in the i_d-i_q-plane. For this analysis the 24th order of the torque is selected,

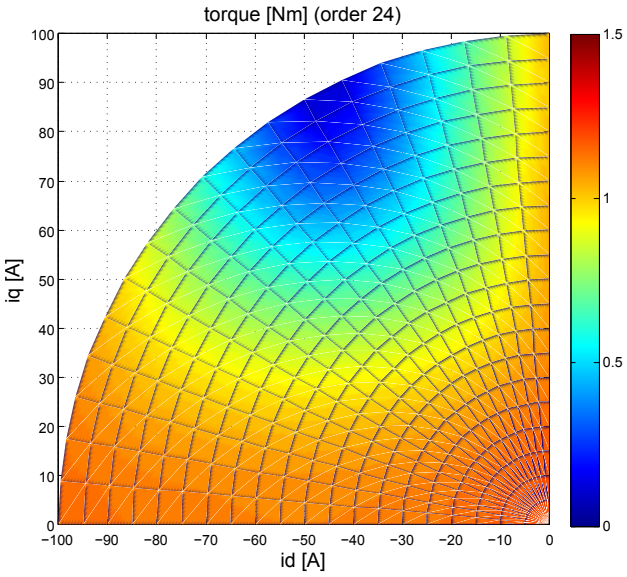

Figure 8. Torque ripple. Order 24 as a function of currents i_d and i_q. Parameter constellation with $\theta_\mathrm{i} = 100°$ and $\theta_\mathrm{a} = 110°$.

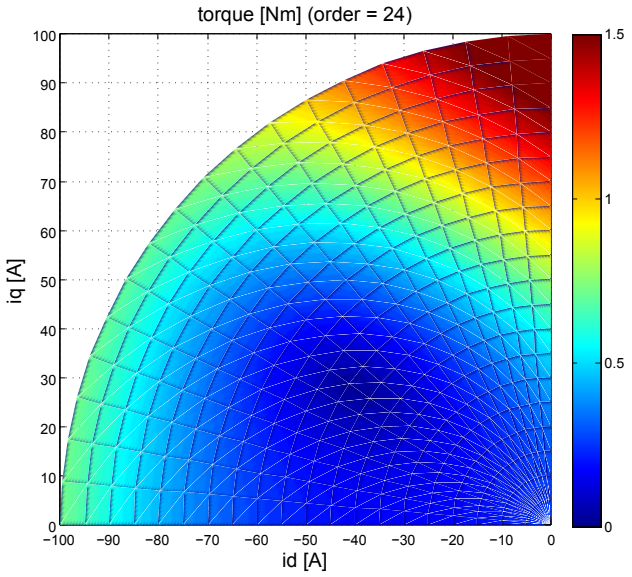

Figure 9. Torque ripple. Order 24 as a function of currents i_d and i_q. Parameter constellation with $\theta_\mathrm{i} = 150°$ and $\theta_\mathrm{a} = 140°$.

Table VIII
RADIAL FORCE DENSITY. STRAIN AMPLITUDE. SURFACE VELOCITY.

radial force density [N/m^2]			
	$\theta_\mathrm{i} = 100°$	$\theta_\mathrm{i} = 150°$	reduction
	$\theta_\mathrm{a} = 110°$	$\theta_\mathrm{a} = 140°$	[%]
time / spatial	amplitude	amplitude	
0 / 0	6863	6398	6.8
0 / 12	3775	3544	6.1
0 /-12	3011	2853	5.2
8 / 0	2399	2240	6.6
-8 / 4	2230	1905	14.6
strain amplitude [nm]			
	$\theta_\mathrm{i} = 100°$	$\theta_\mathrm{i} = 150°$	reduction
	$\theta_\mathrm{a} = 110°$	$\theta_\mathrm{a} = 140°$	[%]
time / spatial	amplitude	amplitude	
0 / 0	3.813	3.525	7.6
8 / 0	1.376	1.261	8.4
surface velocity [μm/s]			
	$\theta_\mathrm{i} = 100°$	$\theta_\mathrm{i} = 150°$	reduction
	$\theta_\mathrm{a} = 110°$	$\theta_\mathrm{a} = 140°$	[%]
time / spatial	amplitude	amplitude	
8 / 0	6.339	5.811	8.3
8 /-4	1.834	1.481	19.2

because it describes the harmonics resulting of the interaction between the permanent magnets and the slots of the stator. In figure 8 the 24th order for the constellation with $\theta_\mathrm{i} = 100°$ and $\theta_\mathrm{a} = 110°$ is shown. In this case the torque ripple is small for the nominal current I=100 A and control angle $\psi = 35°$ and increases at other operating points. In figure 9 the 24th order for another constellation with $\theta_\mathrm{i} = 150°$ and $\theta_\mathrm{a} = 140°$ is shown. In comparison to figure 8 the nominal point is not the most beneficial operating point for this harmonic. For a beneficial design of the flux barrier angles, the operating area of the machine has to be known. By variating the current I and the control angle ψ the torque ripple can be influenced.

VI. EVALUATION OF RADIAL FORCE DENSITY

In this section the radial component of the resulting force density $F_\mathrm{a,rad}$ acting on the stator of the machine is analyzed. The analysis is performed for two constellations of flux barrier angles. The first constellation with $\theta_\mathrm{i} = 100°$ and $\theta_\mathrm{a} = 110°$ is a case of higher torque ripple and low effective torque. The second constellation with $\theta_\mathrm{i} = 150°$ and $\theta_\mathrm{a} = 140°$ produces higher effective torque and lower torque ripple.

A. Resulting radial force density

In table VIII the radial force density, the strain amplitude and the surface velocity are calculated for the above presented constellations of flux barrier angles. Combinations of time and spatial dependent force density orders are chosen and their amplitudes are presented. The strain amplitude describes the deformation of the material at the surface of the machine. The surface velocity represents the speed of this deformation. The calculation is based on an analytical model in [4], which reduces the housing of the machine into an ideal cylinder. For the constellation with larger inner barrier angle $\theta_\mathrm{i} = 150°$ the force density of the order combination (8 / 0) is reduced by 6.6 %. This results in a reduction of 8.3 % in the surface velocity. From this analysis can be concluded, that constellations with large inner flux barrier angle result in lower radial force density harmonics.

B. Evaluation for different operating points

In this section the radial force density $F_\mathrm{a,rad}$ is analyzed for two specific flux barrier angle constellations, which are used in section V ($\theta_\mathrm{i} = 100°/\theta_\mathrm{a} = 110°$ and $\theta_\mathrm{i} = 150°/\theta_\mathrm{a} = 140°$). The radial force density $F_\mathrm{a,rad}$ is calculated for all operating points in the i_d-i_q-plane. In figure 10 the difference of force densities of both constellations is shown. The combination of

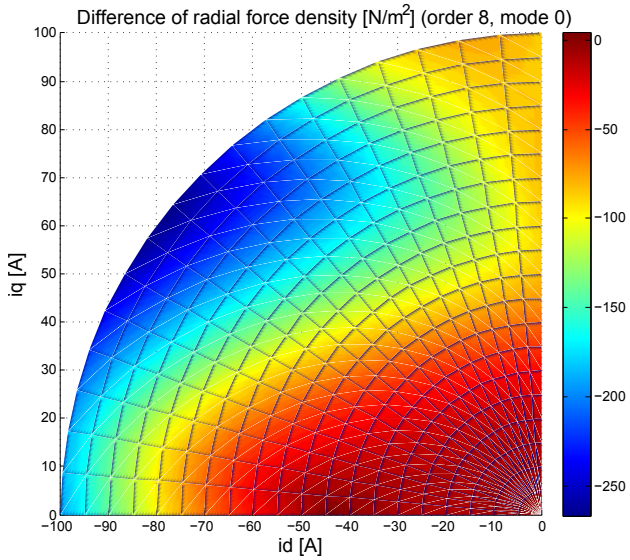

Figure 10. Difference plot of radial force density. Constellation ($\theta_\mathrm{i} = 100°/\theta_\mathrm{a} = 110°$ is subtracted from $\theta_\mathrm{i} = 150°/\theta_\mathrm{a} = 140°$). Time order 8. Spatial order 0.

time order 8 and spatial order 0, which is identified as relevant for the surface velocity (see table VIII), is considered. It is expected that the constellation ($\theta_\mathrm{i} = 150°/\theta_\mathrm{a} = 140°$) results in smaller resulting radial force density, which is observable in every operating point. For operating points near the nominal value this effect is more intense.

VII. Conclusions

The permanent magnet synchronous reluctance machine (PMSynRM) has different design criteria to manipulate the acoustic behavior of the machine. The variation of flux barrier angles and thereby the variation of the magnetic circuit of the rotor has a large influence on this behavior. The presented machine design is evaluated for the air gap flux density, the resulting torque and the radial force density in a combined analysis. For a beneficial acoustic design, the flux barrier angles have to be wide to realize a large pole pitch factor. For the most beneficial constellation a slightly pointed shape form is established, to reduce torque ripple while keeping the resulting effective torque constant. The variant ($\theta_\mathrm{i} = 150°/\theta_\mathrm{a} = 155°$) is preferred. The design approach consists of parameter variation of flux barrier angles and an interpretation of specific operating points for the chosen constellations. The structural dynamic simulation and psycho acoustic analysis will be performed in future work.

References

[1] T. M. Jahns, G. B. Kliman, and T. W. Neumann, "Interior permanent-magnet synchronous motors for adjustable-speed drives," *IEEE Transactions on Industry Applications*, vol. IA-22, no. 4, pp. 738–747, Jul. 1986.

[2] T. Habetler and D. Divan, "Acoustic noise reduction in sinusoidal PWM drives using a randomly modulated carrier," in *, 20th Annual IEEE Power Electronics Specialists Conference, 1989. PESC '89 Record*, 1989, pp. 665–671 vol.2.

[3] G. A. Covic and J. T. Boys, "Noise quieting with random PWM AC drives," *Electric Power Applications, IEE Proceedings* -, vol. 145, no. 1, pp. 1–10, 1998.

[4] H. Jordan, *Geräuscharme Elektromotoren, Lärmbildung und Lärmbeseitung bei Elektromotoren*. W. Girardet, Essen, Germany, 1950.

[5] H. O. Seinsch, *Oberfelderscheinungen in Drehfeldmaschinen, Grundlagen zur analytischen und numerischen Berechnung*. B.G. Teubner Stuttgart, 1992.

[6] J. F. Gieras, C. Wang, and J. C. Lai, *Noise of Polyphase Electric Motors*. CRC Press, Taylor & Francis Group, 2006.

[7] M. Hafner, D. Franck, and K. Hameyer, "Static electromagnetic field computation by conformal mapping in permanent magnet synchronous machines," *IEEE Transactions on Magnetics*, vol. 46, no. 8, pp. 3105–3108, 2010.

[8] X. Bomela and M. Kamper, "Effect of stator chording and rotor skewing on performance of reluctance synchronous machine," *IEEE Transactions on Industry Applications*, vol. 38, no. 1, pp. 91–100, 2002.

[9] S. Rick, M. Felden, M. Hombitzer, and K. Hameyer, "Permanent magnet synchronous reluctance machine - bridge design for two-layer applications," in *Electric Machines Drives Conference (IEMDC), 2013 IEEE International*, May 2013, pp. 1376–1383.

[10] D. J. Ewins, *Modal Testing: theory, Practice and Application*, E. Professor J.B. Roberts, University of Sussex, Ed. Research Studies Press LTD., Baldock, Hertfordshire, England, 2000.

[11] P. Niazi, H. A. Toliyat, D.-H. Cheong, and J.-C. Kim, "A low-cost and efficient permanent-magnet-assisted synchronous reluctance motor drive," *IEEE Transactions on Industry Applications*, vol. 43, no. 2, pp. 542–550, Apr. 2007.

[12] A. S. Ogunjuyigbe, A. A. Jimoh, D. V. Nicolae, and E. S. Obe, "Analysis of synchronous reluctance machine with magnetically coupled three-phase windings and reactive power compensation," *IET Electric Power Applications*, vol. 4, no. 4, pp. 291–303, Apr. 2010.

[13] Y. Honda, T. Higaki, S. Morimoto, and Y. Takeda, "Rotor design optimisation of a multi-layer interior permanent-magnet synchronous motor," *Electric Power Applications, IEE Proceedings* -, vol. 145, no. 2, pp. 119–124, Mar. 1998.

[14] N. Bianchi, S. Bolognani, D. Bon, and M. Dai Pre, "Rotor flux-barrier design for torque ripple reduction in synchronous reluctance and PM-Assisted synchronous reluctance motors," *IEEE Transactions on Industry Applications*, vol. 45, no. 3, pp. 921–928, Jun. 2009.

[15] I. Boldea, L. Tutelea, and C. I. Pitic, "PM-assisted reluctance synchronous motor/generator (PM-RSM) for mild hybrid vehicles: electromagnetic design," *IEEE Transactions on Industry Applications*, vol. 40, no. 2, pp. 492– 498, Apr. 2004.

VIII. Biographies

Sebastian Rick received his Dipl-Ing. degree in electrical engineering from RWTH Aachen University, Aachen, Germany, in May 2012. He has been working as a research associate at the Institute of Electrical Machines of RWTH Aachen University, Germany since June 2012. His research interests include new arts of electrical machines, simulation and acoustical design of electrical machines.

Aryanti Kusuma Putri received the M.Sc. degree in electrical engineering from RWTH Aachen University, Aachen, Germany, in April 2013. She has been working as a research associate at the Institute of Electrical Machines since June 2013. Her research interests include contactless power transmission, new arts of electrical machines, simulation and acoustical design of the electrical machines.

David Franck received the Dipl.-ing. degree in electrical engineering from RWTH Aachen University, Aachen, Germany, in March 2008. After that he became of staff (research associate) at the Institute of Electrical Machines. Since 2011 he has been working as chief engineer of the Institute of Electrical Machines. His main field of research is acoustic of the electrical machines.

Dr. Kay Hameyer received his M.Sc. degree in electrical engineering from the University of Hannover and his Ph.D. degree from the Berlin University of Technology, Germany. After his university studies he worked with the Robert Bosch GmbH in Stuttgart, Germany as a Design Engineer for permanent magnet servo motors and vehicle board net components. Until 2004 Dr. Hameyer was a full Professor for Numerical Field Computations and Electrical Machines with the KU Leuven in Belgium. Since 2004, he is full professor and the director of the Institute of Electrical Machines (IEM) at RWTH Aachen University in Germany. 2006 he was vice dean of the faculty and from 2007 to 2009 he was the dean of the faculty of Electrical Engineering and Information Technology of RWTH Aachen University. His research interests are numerical field computation and optimization, the design and controls of electrical machines, in particular permanent magnet excited machines, induction machines and the design employing the methodology of virtual reality. Since several years Dr. Hameyers work is concerned with the magnetic levitation for drive systems, magnetically excited audible noise in electrical machines and the characterization of ferromagnetic materials. Dr. Hameyer is author of more than 250 journal publications, more than 500 international conference publications and author of 4 books. Dr. Hameyer is a member of VDE, IEEE senior member, fellow of the IET.